Localized mechanical stress induced ionic redistribution in a layered $LiCoO_2$ cathode

Wentao Yao[1], Fei Long[1], Reza Shahbazian-Yassar[1,2]*

1. Department of Mechanical Engineering-Engineering Mechanics, Michigan Technological University, 1400 Townsend Drive, Houghton, Michigan 49931, United States

2. Department of Mechanical and Industrial Engineering, the University of Illinois at Chicago, Chicago, Illinois 60607, United States

KEYWORDS: *$LiCoO_2$, conductive AFM, stress, ionic redistribution, resistive switching*

ABSTRACT: Controlling the transport of ions within electrodes is highly desirable for the operation of rechargeable ion batteries. Here, for the first time, we report the role of mechanical stress in controlling the redistribution of lithium ions in a layered $LiCoO_2$ electrode at a resolution of ~100 nm. Under higher stress field, more active redistribution of lithium ions was observed along the grain boundaries than the interiors of the layered $LiCoO_2$. The dynamic force ramping test proved the external stress field (<100 nN) is capable of inducing the resistive-switching effect of the layered $LiCoO_2$. The comparison test on the highly ordered pyrolytic graphite (HOPG) substrate further demonstrated the improved current responses from the layered $LiCoO_2$ were resulted from the deficiency of lithium ions, rather than the increase of tip-sample

contact area. Our findings will pave the road for a full understanding of how mechanical stimulus can affect the distribution of ions in the layered electrodes of rechargeable ion batteries.

1. INTRODUCTION

Lithium-ion batteries have been widely used as power sources for portable electronic devices as well as hybrid vehicles.[1-3] To meet the future demand for energy storage, improvements in charge capacity and power density are still needed.[4] Nanostructured electrode materials have shown promising potential in improving the performance of lithium-ion batteries, because they offer higher contact area, increased lithium intercalation rate, and shorter electron pathways.[5] To improve the understanding of the relationship between the nanostructures and their electrochemical performance, nanoscale studies are needed with the help of high-resolution microscopes.[6-9]

Layered $LiCoO_2$ is the most widely used and commercialized cathode material for lithium-ion batteries due to its relatively high capacity and excellent stability.[10-11] Under a concentrated electric field, the lithium ions tend to be driven away from the slabs of CoO_2 octahedral structures, resulting in localized deficiency of lithium ions.[8] The deficiency of lithium ions further induces two major changes inside the $LiCoO_2$ electrode: lattice expansion along its *c*-axis and resistive switching from semi-conductive to metallic state.[12-14] The lattice expansions along the *c*-axis (Li_xCoO_2, $0.5 < x < 1$)[15] are detectable using atomic force microscopy (AFM). Based on this dimensional change, Balke, *et al* successfully developed electrochemical strain microscopy (ESM) to study the distribution of lithium ions inside layered $LiCoO_2$ under both direct and alternating bias voltages.[8] The resistive switching phenomenon is related to the electromigration of ions and electrochemical reactions. This phenomenon was also observed with other cations (Cu^{2+}, Ag^{+} or Ni^{2+})[16-18] and substrates[19] other than layered $LiCoO_2$. Using

conductive AFM (C-AFM), the resistive switching effect can be revealed based on the current responses from the substrate under a bias voltage. The obtained current mapping image can be used to visualize the redistribution of lithium ions. Using C-AFM, Zhu, *et al* proved more active redistribution of lithium ions along $LiCoO_2$ grain boundaries than the interiors and further demonstrated the energy barrier for the diffusion of lithium ions is lower along the boundaries.[20] Other influencing factors for the redistribution of lithium ions inside the layered $LiCoO_2$ cathode, such as temperature[21] and grain orientation[22], have been studied at the nanoscale using ESM.

Under a positive electric field, the internal mechanical strain is generated as a result of the expansion along the *c*-axis of the layered $LiCoO_2$ cathode because of the deficiency of lithium ions. This is similar to the piezoelectric effect, where the applied electric field can generate internal mechanical strains. This process is mainly reversible for piezoelectric materials. However, for layered $LiCoO_2$, whether external mechanical stress can regulate the redistribution of ions has never been studied. In this report, commercial layered $LiCoO_2$ substrate was used to study the effect of localized stresses on the redistribution of lithium ions under a constant electric field. High-resolution tunneling current module (TUNA) was adopted for C-AFM tests to reach a high current resolution (<1pA). The effect of external stresses on the resistive switching of layered $LiCoO_2$ was also studied by a dynamic force ramping technique.

2. METHODS

2.1 Materials. The $LiCoO_2$ thin film was purchased from MTI Corp and used as received. The thickness of the film was 0.1mm and coated on an aluminum foil. The scanning electron microscopy (SEM) image was obtained from a Hitachi S-4700 Field Emission scanning microscope under an accelerating voltage of 10 kV. X-ray powder diffraction (XRD) pattern was obtained from a Scintag XRS2000 powder diffractometer using Cu $K\alpha_1$ radiation with a step size

of 0.02°. The HOPG sample was obtained from the standard sample kit offered from Bruker Company. The thickness of the HOPG sample is around 2 mm and mounted on a steel plate using conductive polymer.

2.2 C-AFM test. All C-AFM tests were carried out using the Dimension ICON system (Bruker, CA.) under ambient conditions. Conductive AFM probes (Multi75E-G, budget sensors) with double-sided Pt/Ir coating were used. The length and width of the probe cantilever are 225 μm and 28 μm, respectively. The TUNA external module (Figure 1a) was used to provide high current sensitivity. The offset and gain adjustments were performed for the TUNA module before the C-AFM tests. Specific 100 Mega Ohms dummy resistor was used for the gain adjustment. The current sensitivity used was set to 100 nA/V during the tests. The bias voltage was added to the substrate as illustrated in Figure 1a. Under the C-AFM mode, the AFM probe was kept in contact with the substrate to obtain the current response.

2.3 Calibration of deflection sensitivity and spring constant. For the calibration of deflection sensitivity, a sapphire sample (Young's modulus 345 GPa, from the standard AFM sample kit) was used to ensure enough stiffness and reduce the influence of surface deformation. Average deflection sensitivity of the system was obtained from sensitivity values generated from five different spots on the sapphire sample. The sensitivity test was repeated three times at each spot. Spring constants of the probes were calibrated using the Sader method.[23] The spring constant is determined by its resonance frequency, Q factor, and geometry. The value of resonance frequency and Q factor were obtained under the tapping mode before the C-AFM test.

2.4 Dynamic force ramping. The dynamic force ramping was realized by ramping the distance (***Z***) between the substrate and the cantilever rest position instead. Under C-AFM mode, the ***Z*** value was ramped with a ramp size of 250 nm and a ramp rate of 0.3 Hz. The forward and

retract velocities of the probe were kept the same at 145 nm/s. Once the relationship between $\boldsymbol{Z}$ value and current response was obtained, the $\boldsymbol{Z}$ value can be transformed into its corresponding applied force by using the force-distance curves generated on the substrate. Under contact mode, the tip-sample distance equals zero, thus the distance between the substrate and the cantilever rest position ($\boldsymbol{Z}$) is equal to the deflection of the cantilever, which is proportional to the force applied on the substrate according to the Hooke's Law.

2.5 Forces calibration. Adjusting the forces applied through the AFM probe controls the mechanical stress applied to the substrate. Under the C-AFM mode, the probe stays in contact with the substrate. Actual forces applied on the substrate can be calibrated based on the deflection of the cantilever according to the Hook's law.[24] The cantilever deflection can be calculated based on the setpoint value and the deflection sensitivity of the probe. The applied force can be determined by multiplying the value of setpoint (V), the deflection sensitivity of the system (nm/V), and the spring constant of the probe (N/m). For the probes used on different substrates, the calibrated parameters are shown in Table 1. Assuming the deflection sensitivity of the system and spring constant of the probe were constant during the test, the applied forces can be considered as proportional to the setpoint value. Thus, the stress loading process can be realized by increasing the setpoint value from 0.1 to 0.8 V with a step size of 0.1 V. The unloading process was conducted with the same step size but changing the setpoint value from 0.8 to 0.1 V. The setpoint value was limited to 0.8 V to prevent the probe from damaging the substrate.

Table 1 Calibrated parameters of the AFM probes used on different substrates

Substrate	Deflection sensitivity (nm/V)	Probe characteristics	
		Resonance frequency (kHz)	Spring constant (N/m)
$LiCoO_2$	117.5 ± 3.2	66.87	2.24 ± 0.05
HOPG	107.4 ± 0.5	73.95	2.48 ± 0.05

3. RESULTS AND DISCUSSION

3.1 C-AFM tests on the layered $LiCoO_2$ cathode. The topography image in Figure 1b and SEM image (See Supporting Information, Figure S1) show a layered and polycrystalline structure of the $LiCoO_2$ thin film. The XRD diffraction peaks (Figure S2) are in good agreement with rhomb-centered O_3-$LiCoO_2$ (JCPDS 16-0427). Minor peaks at 37.4° and 44.4° can be indexed to Co_3O_4 (JCPDS 80-1544), which shall come from the manufacturing process. The peak intensity ratio also fits well with the standard, indicating no preferred growth direction for the $LiCoO_2$ substrate. The applied DC voltage was selected at 2V to ensure the resistive switching effect can be generated.[14] Electric current mapping under different localized stress is shown in Figure 1c. The upper row in Figure 1c shows the stress loading process (setpoint at 0.1, 0.3, 0.5, and 0.7 V, respectively), while the lower row shows the stress unloading process. The bright areas in the electric current mapping image indicate conductive regions on the substrate. During the stress loading process, under an applied force of 26.3 ± 1.1 nN (setpoint at 0.1 V), a low electric current contrast was observed between the boundaries and the grain interiors. Further increasing the applied force to 78.9 ± 3.2 nN (setpoint at 0.3 V) caused the conductive regions to expand and these conductive regions mainly distributed along the grain boundaries. During the unloading process, the area of conductive regions and the intensity of electric current output reduced along with the decrease of applied stress. The electric current responses under the

26.3 ± 1.1 nN and the 78.9 ± 3.2 nN applied forces were slightly higher than that during the loading process. This is related to the hysteresis effect from the loading process.[25]

Under the DC voltage of 2V, some areas of the substrate were still in a non-conductive state. This indicated that the lithium ions were not completely driven away by the external electric field. The resistive switching of Li_xCoO_2 happens when the lithium composition is in the range of $0.75 \leq x \leq 0.94$.[12] The observed electric current distribution along grain boundaries is consistent with the work from Zhu *et al* [20]. Instead of even distribution of current response along all boundary areas, some boundary areas did not show electric current responses in our case. This is due to the polycrystalline structure of the $LiCoO_2$ substrate; different grains are oriented in different directions. The diffusion of lithium ions is only preferred along the (001) planes, between the adjacent CoO_2 layers.[8] The redistribution of lithium ions is maximized when the orientation of the layered structure is parallel to the external electric field, because of the high mobility of the lithium ions and possible surface reactions.[22] When the layered Li-ion/CoO_2 planes are aligned normally to the electric field, the redistribution of lithium ions would be minimized, but strong out-of-plane volume change along the *c*-axis can be observed. Because of the different orientations of the layered $LiCoO_2$ grains, dissimilar electrical current responses can be detected at the boundaries (Figure S3). In our case, the AFM scan direction and sample position were kept the same all the time, so grain orientations did not affect our comparison among different electrical current signals.

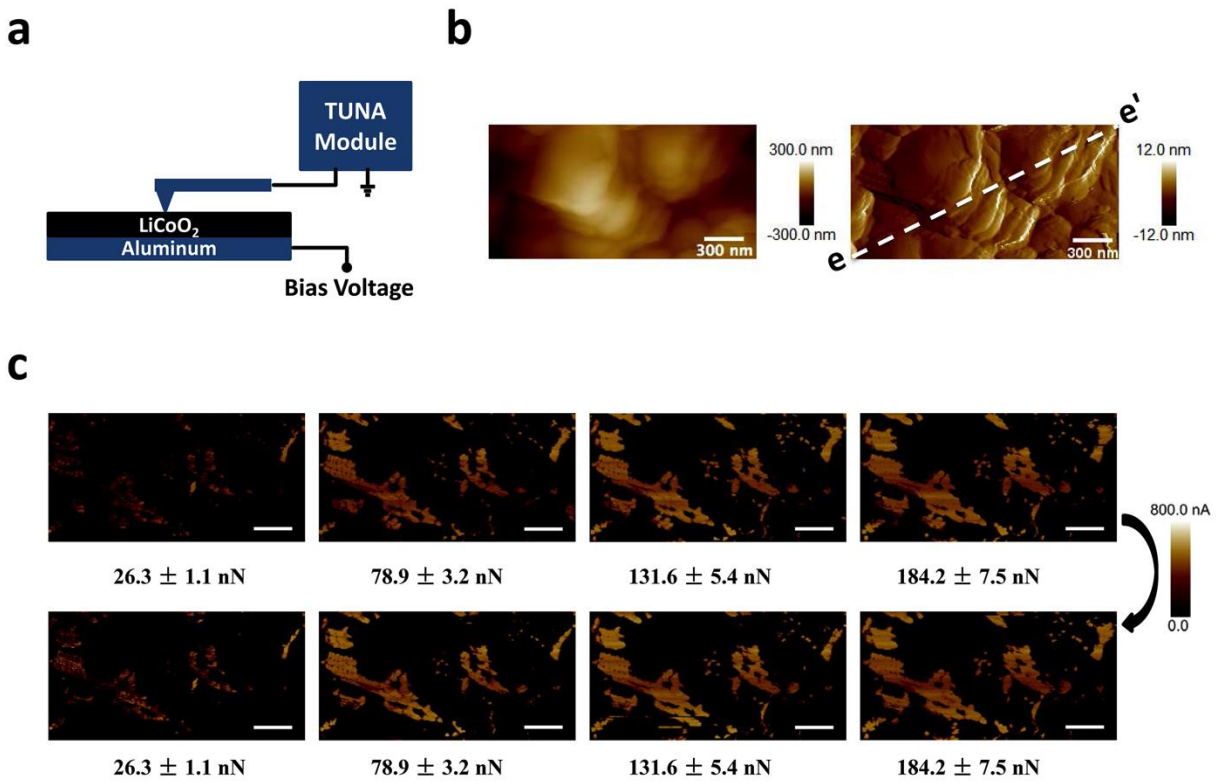

Figure 1. (a) A schematic image of the C-AFM test setup with TUNA module. (b) Height (left) and deflection (right) images of the $LiCoO_2$ substrate. The dashed line (e-e') is for the section analysis discussed in Figure 2b. (c) Electric current mapping of the corresponding area during the stress loading (upper row) and unloading processes (lower row) under 2 V bias voltage. Scale bars are 300 nm.

For quantitative analysis of the current response, arithmetic mean roughness (R_a) and the root-mean-square roughness (R_q) of the current signal were analyzed. Under the bias voltage of 2V, the R_a value increased nonlinearly from 43.6 to 183.0 nA when the external force was increased from 26.3 nN to 210.5 nN (Figure 2a). For a better understanding of the effect of stress field on Li-ion redistribution, C-AFM tests without bias voltages were also performed at the same time under the same loading/unloading conditions (Figure S4). To reduce any possible hysteresis effect from the electric field, C-AFM tests without the bias voltage were performed before the

tests with the 2V DC voltage. When the electric field is removed (0V), the R_a value increased from 0.0135 to 0.0254 nA under the same loading condition. The current observed from the regions with Li-ion deficiency was negative, which was due to the negatively charged CoO_2 layers after the interlayer lithium ions were driven away by external stresses. The detected current flow maybe was induced by the potential differences between the negatively charged CoO_2 layers and the redistributed lithium ions. This demonstrated that mechanical stress is capable of inducing lithium ions redistribution with or without the electric field. The similar trend was observed with the change of the R_q value versus external stress (Figure S5). The increase of R_a and R_q values indicate more conductive regions were induced by the enhanced external stress. The average value of the current output is identical during both loading and unloading processes, indicating a relatively reversible effect of the external stress field on the current response at the level of a few hundred nano-newtons. The increasing rate of the R_a value reduced along with the improving of applied forces. The decrease of this rate indicates the slowing down of the distribution of lithium ions. It is possible that this stress-induced lithium ion redistribution may be limited to some extent. The effect of external stress on redistribution of lithium ions was weakened with the depletion of lithium ions inside its layered structure.

Based on the cross-section analysis results (Figure 2b), when the applied external stress field was increased, an expansion of the conductive regions was observed, indicating larger areas of the layered $LiCoO_2$ switched from a semi-conductive state to a metallic state. The sharp current peaks along the conductive regions are consistent with the resistive switching phenomena of the layered $LiCoO_2$ cathode. The two dashed lines g and g' were drawn to show the change of current response inside the conductive region along with the increase of the external stresses. Clearly, the magnitude of the electric current response increased inside the g-g' region. This

demonstrated that adding more stresses increased the redistribution of lithium ions inside the conductive regions.

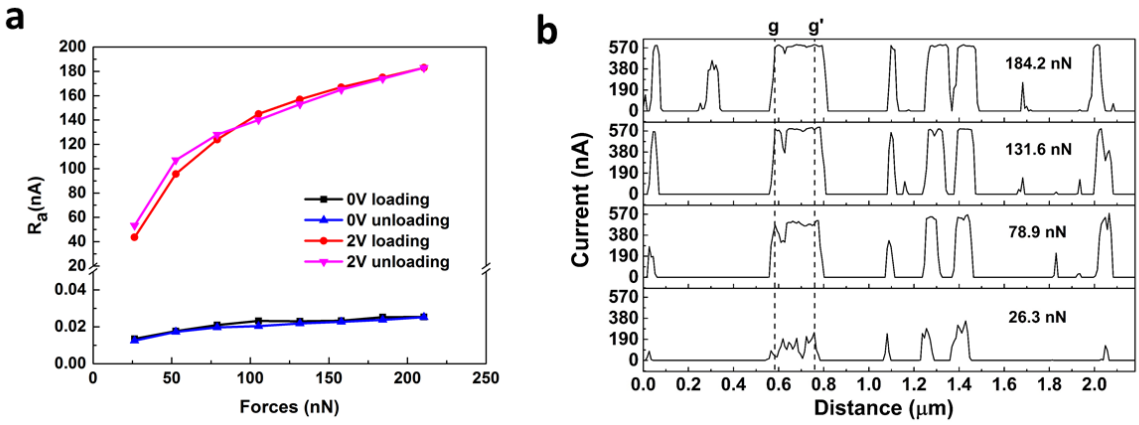

Figure 2. (a) Arithmetic mean roughness (R_a) of electric current output from the $LiCoO_2$ thin film as a function of applied forces under 0V and 2V bias voltage. (b) Cross section along the diagonal line e-e' in Figure 1b for the current signals during the stress loading process. Dashed lines g and g' were drawn for comparison of the current signals from the same location.

To compare the scan rate with the diffusion rate of lithium ions, further experiments were conducted. The scan rate used for obtaining C-AFM images (Figure 1c) was 3.2 μm/s (0.8Hz). Three C-AFM images (Figure S6) were obtained consecutively at the same location under the same scan rate of 3.2 μm/s (0.8 Hz) and the same bias voltage of 2V. Figure S6b was obtained immediately after Figure S6a under the same condition. No obvious contrast change was observed, indicating fast and stable current response from the substrate. Figure S6c was obtained soon after Figure S6b with an increase in applied force to 52.6 nN while keeping other parameters the same. When the applied force was increased, a higher contrast was observed immediately. This demonstrates that the redistribution of lithium ions is faster enough than our scan rate, and thus will not affect our current mapping.

3.2 Dynamic force ramping on the layered $LiCoO_2$. To further study the influence of external stress field on the redistribution of lithium ions at different parts of the layered $LiCoO_2$ cathode, the dynamic force ramping was performed and representative force-current curves were obtained from five different spots on the $LiCoO_2$ substrate, as shown in Figure 3a. Spot 1 and Spot 2 were located in the interior of the $LiCoO_2$ grains, while Spot 3, 4, and 5 were located along different grain boundaries.

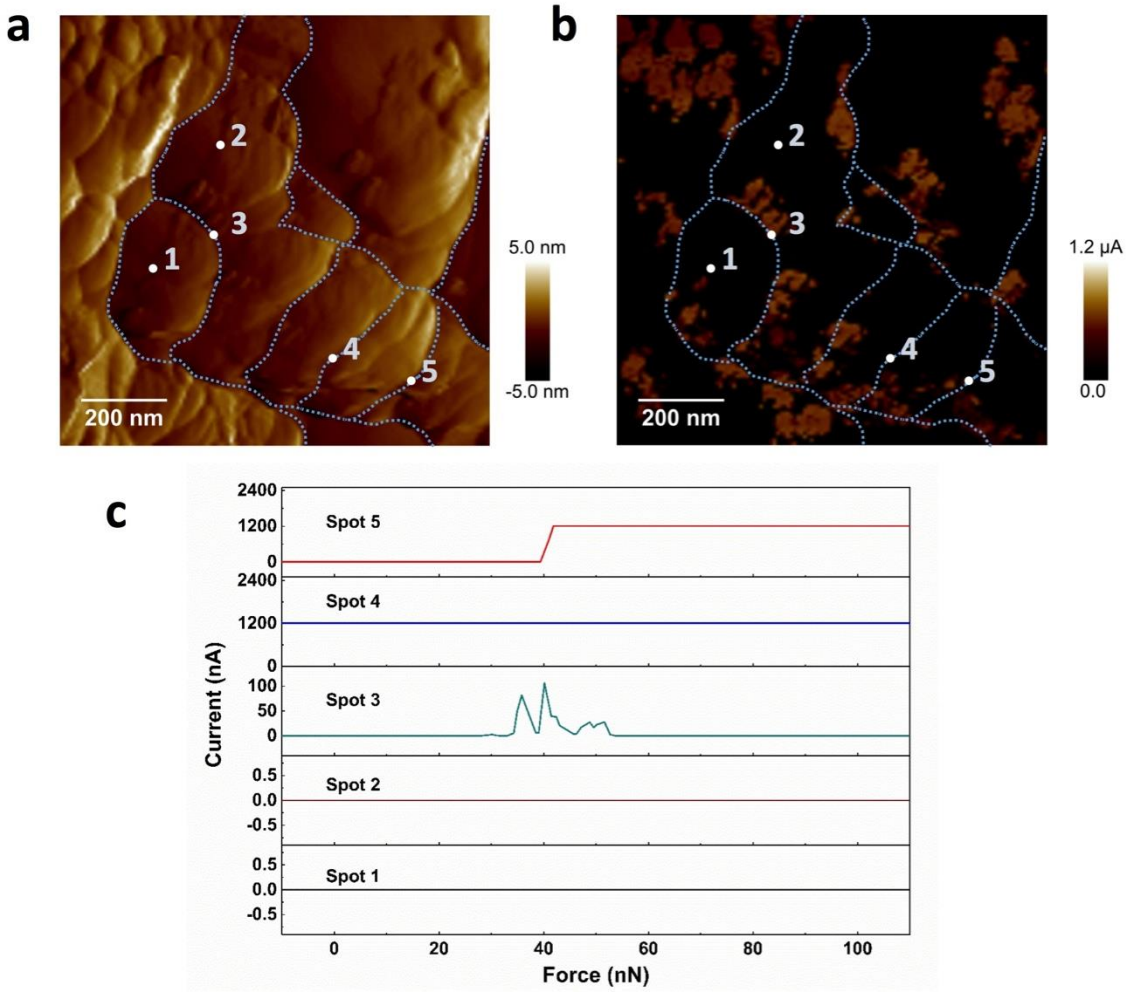

Figure 3. Deflection (a) and TUNA current output images (b) obtained on the $LiCoO_2$ substrate under a bias voltage of 2V. Blue dashed lines were drawn to indicate different grain boundaries. (c) The representative force-current curves obtained from five different spots respectively.

The same kind of conductive probe was used for the dynamic force ramping test. The calibrated deflection sensitivity was 108.9 ± 2.0 nm/V and the calibrated spring constant was 2.65 N/m. Obtained relationships between applied forces and current responses are shown in Figure 3c. The electric current map in Figure 3b shows a positive current output along the grain boundaries. The force applied to obtain Figure 3b was 28.8 ± 2.0 nN. Although the ramp size was 250 nm, dynamic forces applied on the $LiCoO_2$ substrate were only effective in the range of 0 ~ 110 nN (Figure 3c). The current responses detected during the tip retracting were used to study their relationship with the applied forces.

Spot 1 and 2 were located inside the grain interiors and showed an insulator behavior, indicating a reluctant redistribution of lithium ions inside the grain interiors. The behavior of the two spots is consistent with the nonconductive regions in Figure 2b ("valleys" of the graph). Spots 4 and 5 were located along the layered grain boundaries. Spot 4 showed a pure conductive behavior, indicating a high deficiency of lithium ions inside this region, which is consistent with the conductive regions in Figure 2b ("peaks" of the graph). The 1.2 μA platform is actually the detection limit of the TUNA module. Spot 5 switched from a semi-conductive state to a conductive state when the applied force reached around 40 nN. This region remained conductive when the applied force was further increased up to 110 nN. The conductivity change was shown to be reversible during the tip trace and retrace process (Figure S7). This behavior is also consistent with the step-by-step stress loading-unloading condition, indicating reversible resistive switching induced by external stresses. Although Spot 3 is also located at the grain boundaries, the current output did not show obvious resistive switching. When applied force reached 30 ~ 50 nN, a few current peaks were observed at Spot 3. These current peaks are resulted from possible

electrochemical reactions within the water meniscus at the probe/substrate contact area[14, 26-27] other than resistive switching of the $LiCoO_2$ substrate itself.

The change of current response versus applied stresses at Spot 5 looks different from the trend observed in Figure 2a, where a slight increase was observed instead of a sharp resistive switching peak. This is because Figure 2a offers the variation of averaged current response (R_a) from a scanning area of 2 μm^2 instead of individual spots. By adding more stresses, a larger region of the $LiCoO_2$ substrate will switch to the conductive state, which will result in an increase in the averaged current value. But the conductive spots may remain conductive and give the same current response even under higher stress field. During the step-by-step loading condition, the detection limit (1.2 μA) was not reached over 110 nN. This may be related to the different grain orientations because the two tests were conducted in different areas. On the other hand, different loading methods were used. For the dynamic loading condition, other than the energy from the applied stresses, the kinetic energy of the probe will also accumulate, get absorbed by the substrate and further facilitate the redistribution of lithium ions.

Representative I/V curves from the grain interiors and boundaries of the layered $LiCoO_2$ substrate were also acquired (Figure S8). The grain interiors showed clearly a semiconductor behavior (Figure S8b), and higher threshold voltage was observed at the spots further away from the boundaries. The grain boundaries showed a highly conductive behavior, indicating lower energy barrier for the diffusion of lithium ions.

In sum, the applied external stress (<100 nN) is able to induce reversible redistribution of lithium ions under certain electric fields. Comparing the current output at Spot 1 and Spot 2 with that at Spot 4 and 5, the grain boundaries showed more active redistribution of lithium ions than the grain interiors. The result is identical with previous studies that the Li-ion diffusion barrier

along the grain boundaries is 0.7 eV, which is relatively low compared with diffusion barrier of 6.8 eV in the interiors.[20]

3.3 Comparison C-AFM test on the HOPG. From the electric current mapping on the layered $LiCoO_2$, higher current responses were observed under higher applied stresses. However, with the increase of the applied stresses, the tip-sample contact area would also increase, which could reduce the tip-sample contact resistance[28] and further increase the current output. To determine the influence of tip-sample contact area on the electric current output, a control C-AFM test was performed on the HOPG substrate. HOPG offers smooth and renewable surfaces, which are excellent for AFM tests.

Unlike the ionic conductor $LiCoO_2$, natural layered HOPG is an electron conductor, with an in-plane resistance of 55~65 μΩ·cm and 6~7 mΩ·cm resistance along the *c*-axis.[29] Because of the higher resistance along the *c*-axis, a higher current output can be expected along the boundaries of the HOPG. During both the loading and unloading processes, the C-AFM images (Figure 4c) showed a slight increase in the electric current output when the applied force was increased. Increase in the current output was not only observed along the step edges of the graphite but also appeared to be increased everywhere (Figure S9). The same roughness analysis was conducted for the electric current signals (Figure 5). When the applied force was increased from 26.6 ± 1.1 to 213.1 ± 8.7 nN, the R_a value of the electric current increased from 0.097 to 0.79 nA. The corresponding R_q value also gave a similar trend (Figure S10).

The current response observed from the HOPG sample was lower than that from the $LiCoO_2$ sample. This is because the measured resistance between the HOPG substrate and the AFM sample stage was 1.8 MΩ, which is higher than that of the $LiCoO_2$ sample (0.8 MΩ before its resistive switching). The observed high resistance across the HOPG sample was due to the larger

sample thickness (2mm vs. 0.1mm) and the introduce of the steel plate (vs. aluminum foil under $LiCoO_2$). To keep the current output within the detection limit of the TUNA module and to ensure the effect of tip-sample contact areas can be revealed, this high resistance state across the HOPG substrate was kept during the C-AFM tests. Because the HOPG substrate was in direct contact with the AFM tip and there was no ionic contribution within the electric circuit, the effect of tip-sample contact area can be evaluated.

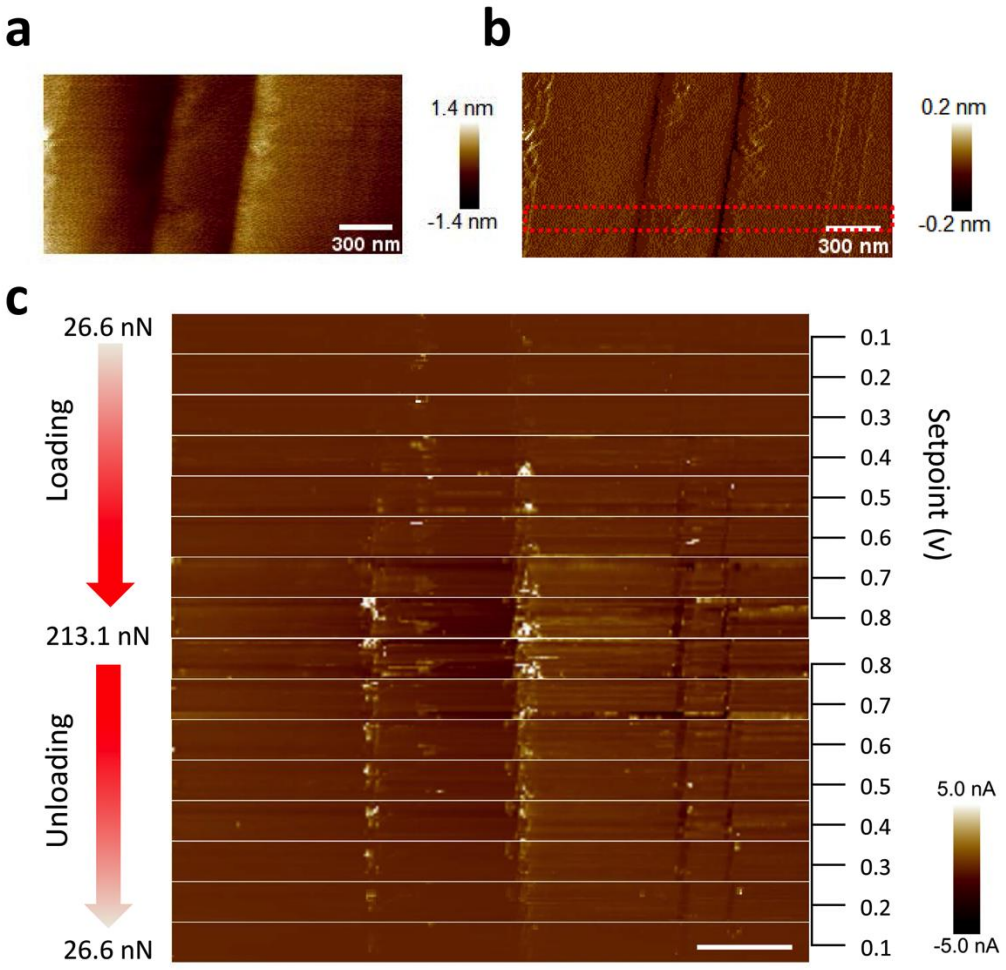

Figure 4. (a) Height and (b) deflection maps of the HOPG substrate under a bias voltage of 2 V, (c) Electric current mapping under different localized forces during loading and unloading processes inside the red dashed box in (b). The scale bars are 300 nm.

The HOPG sample is a relatively soft substrate compared with the AFM probe. The Young's modulus and Poisson's ratio of the silicon tip are estimated to be 169 GPa[30] and 0.22.[31] However, the Young's modulus and Poisson's ratio of the HOPG substrate are 30 GPa[32-34] and 0.24,[34] respectively. Assuming no extra surface forces and low stiffness, the Sneddon analysis model [25] can be adopted to define the relationship between the tip-sample contact radius (***a***) and the applied force (***F***):

$$F = \frac{3}{8}K\left[\left(a^2 + R^2\right)\ln\left(\frac{R+a}{R-a}\right) - 2aR\right] \tag{1}$$

In Equation (1), ***F*** is the applied force, ***R*** is the tip radius (25 nm), and ***K*** is the reduced Young's modulus given by:

$$\frac{1}{K} = \frac{3}{4}\left(\frac{1-\upsilon^2}{E} + \frac{1-\upsilon_i^2}{E_i}\right) \tag{2}$$

where ***E***, E_i, ***v*** and v_i are the Young's modulus and Poisson's ratios of the silicon tip and the HOPG substrate. The reduced Young's modulus of HOPG was calculated to be 35.43 GPa.

Assuming that there is no existence of insulating films between the tip and the substrate and that the electric contact is in a circular area with a radius ***a***, according to Maxwell's theory,[28] the constriction resistance C_r can be given by

$$C_r = (r_1 + r_2)/2a \tag{3}$$

where r_1 and r_2 are the specific resistivity of the two materials in contact. The resistivity of the Pt/Cr coated silicon probe is estimated to be 3.0×10^{-7} Ω·m,[35] and the resistivity of HOPG along the *c*-axis is 3.8×10^{-3} Ω·m.[36] If the current output ***I*** follows Ohm's law under the bias voltage ***U*** = 2V, the relationship between the current output ***I*** and the applied forces ***F*** can be defined as:

$$F = \frac{3}{8}K\left[\left(\frac{I^2(\rho_1+\rho_2)^2}{4U^2}+R^2\right)\ln\left(\frac{2UR+I\rho_1+I\rho_2}{2UR-I\rho_1-I\rho_2}\right)-\frac{IR(\rho_1+\rho_2)}{U}\right] \quad (4)$$

The experimental value was fitted using Equation 4, while the reduced Young's modulus ***K*** was kept as the unknown parameter for a nonlinear curve fitting. The two fitted curves gave an estimate ***K*** value of 35.6 GPa, which is comparable to the theoretical value of 35.43 GPa. The coefficients of determination for the two fitting curves are 0.9009 and 0.9226, indicating the Sneddon model is suitable for our analysis.

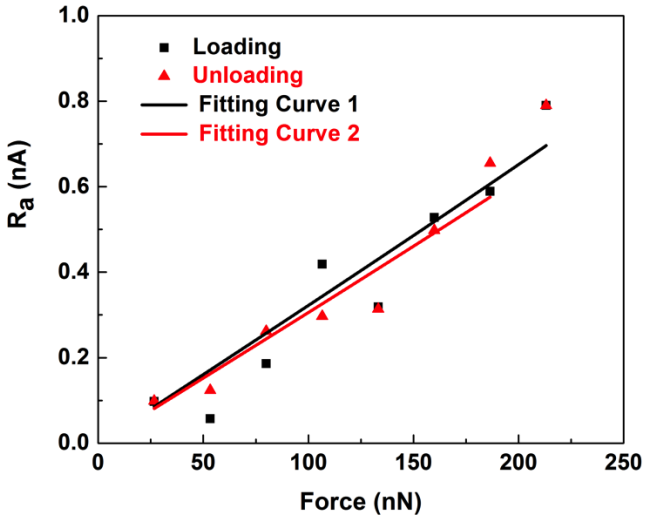

Figure 5. Arithmetic mean roughness (R_a) of the electric current as a function of applied forces on the HOPG substrate. Fitting curve 1 corresponds to loading, and fitting curve 2 corresponds to unloading.

The Young's modulus of layered $LiCoO_2$ is 174 GPa ± 25 GPa, measured from individual grains.[37] Compared with the HOPG substrate, the layered $LiCoO_2$ cathode has a higher hardness. Thus, the corresponding reduced Young's modulus should be higher according to Equation 2. Since the same kind of probe was used for both substrates, under similar loading condition, the tip-sample contact area on the $LiCoO_2$ substrate would be smaller than that on the HOPG

substrate, according to Equation 1. Thus, the effect of tip-sample contact area on the current output would also be smaller on the $LiCoO_2$ substrate. On the other hand, the current increase on the HOPG substrate (1.15 nA increase from 0.268 nA to 1.42 nA) is relatively limited compared with that on the $LiCoO_2$ (139.4 nA increase from 43.6 to 183.0 nA) under the same electric field. Therefore, the effect of tip-sample contact area on the electric current output would be limited and ignorable for the $LiCoO_2$ substrate. The increase in current response on the $LiCoO_2$ substrate should be mainly due to the redistribution of lithium ions.

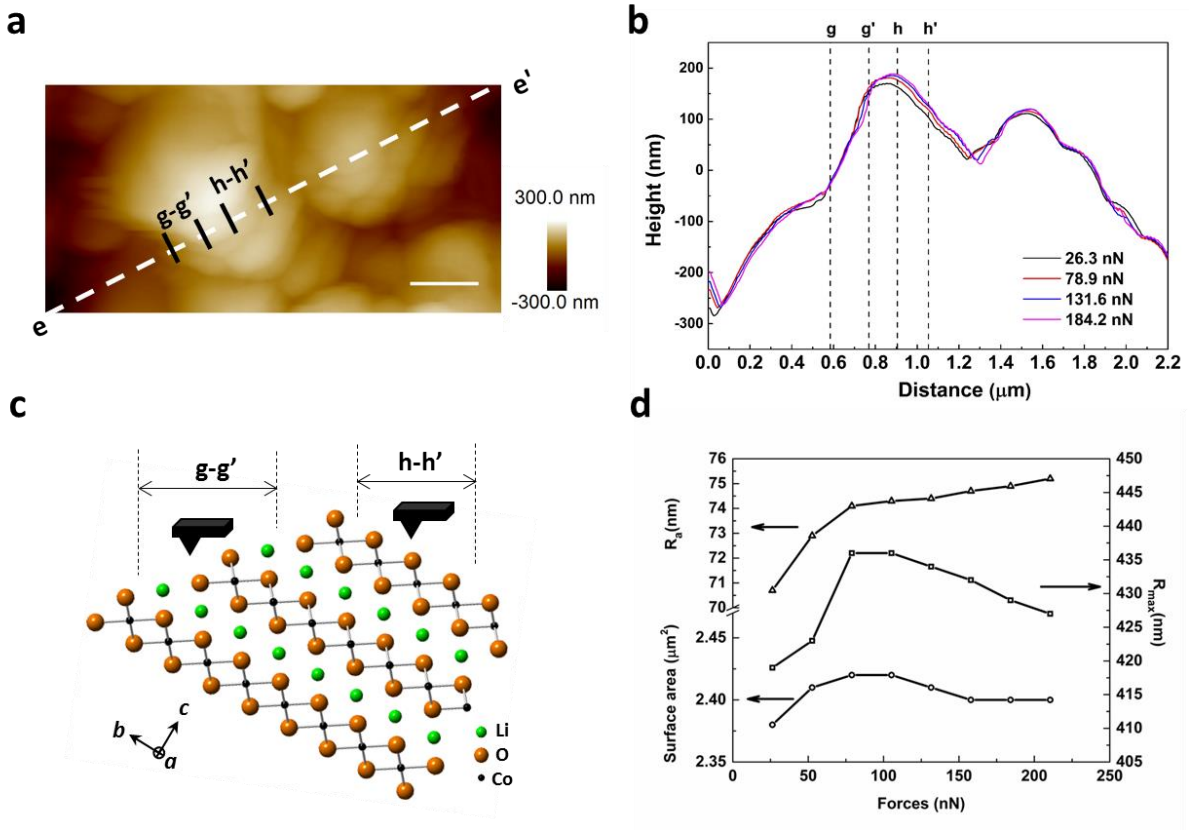

Figure 6. (a) Height image and (b) cross-section analysis of the layered $LiCoO_2$ along the same diagonal line e-e' as Figure 2b during the loading process. The scale bar is 300 nm in Figure 6a. (c) An atomic model of the layered $LiCoO_2$ with a proposed orientation at the g-g' and h-h' locations. (d) Variation of height roughness (R_a and R_{max}) and the surface area of the layered $LiCoO_2$ as a function of applied forces.

To develop a better understanding of the stress-induced redistribution of lithium ions, detailed analysis of the morphology change on the $LiCoO_2$ substrate was also conducted. The topography changes as a function of applied stress were shown in supporting information Figure S11. The obtained topography images were stable, indicating no sample damaged was involved. Compared with the cross-section analysis of the current signals (Figure 2b), the conduction region g-g' showed no obvious surface expansion, which may indicate this grain is oriented with its (001) plane close to the direction of electric field, proposed in Figure 6c. Therefore, minimum expansion or even reduced surface height was observed (Figure 6b). For the region h-h', it belongs to the same layered $LiCoO_2$ grain with the region g-g'. Although no current output was observed, obvious volume expansion was detected. Since these two regions were in the same grain, it is highly possible that the volume expansion detected along the h-h' region was due to the redistribution of lithium ions inside the g-g' region, with a grain orientation proposed in Figure 6c. With the increase of applied forces, the volume expansion at the h-h' region increased, which should be related to the enhanced redistribution of lithium ions at the g-g' region.

The resistive switching of the layered $LixCoO_2$ happens with a lithium concentration within the range of $0.75 \leq x \leq 0.94$, where the diffusion of lithium ions is preferred through the intermediate oxygen-tetrahedral sites (***P₂***) other than a direct jump between two lithium octahedral sites (***P₁***) (Figure S12).[38] The transformation mechanism from $LiCoO_2$ to $Li_{0.75}CoO_2$ was proposed to be an ordering of lithium atoms and vacancies within the (001) lithium layers.[39] The overall dimension of the layered $LiCoO_2$ crystals does not change based on in situ XRD analysis[15] and the theoretical modeling[39]. Previous modeling work also proved stress-enhanced diffusion of lithium ions, rather than diffusion-induced stress, will dominate at a high lithium concentration in amorphous lithium alloy nanowires.[40] In our case, the applied external stress

may facilitate the diffusion of lithium ions or vacancies and further result in resistive switching of the layered $LiCoO_2$. The diffusion of vacancies driven by the stress gradient has also been observed in other semiconductors[41] and alloys[42].

For the further transformation from $Li_{0.75}CoO_2$ to $Li_{0.5}CoO_2$, only one hexagonal phase exists and the substrate will be in a conductive state, similar to that observed along the region g-g'. Along with the further delithiation, a lattice expansion along *c*-axis has been observed[15], which is consistent with that observed at the h-h' region. When lithium ions are driven away from their original location, leaving two negatively charged CoO_2 layers facing each other. The electrostatic repulsions between the two negatively charged CoO_2 layers will induce lattice expansion along the *c*-axis of the layered $LiCoO_2$.[15] Therefore, increased roughness (R_a) and surface area were observed (Figure 6d).

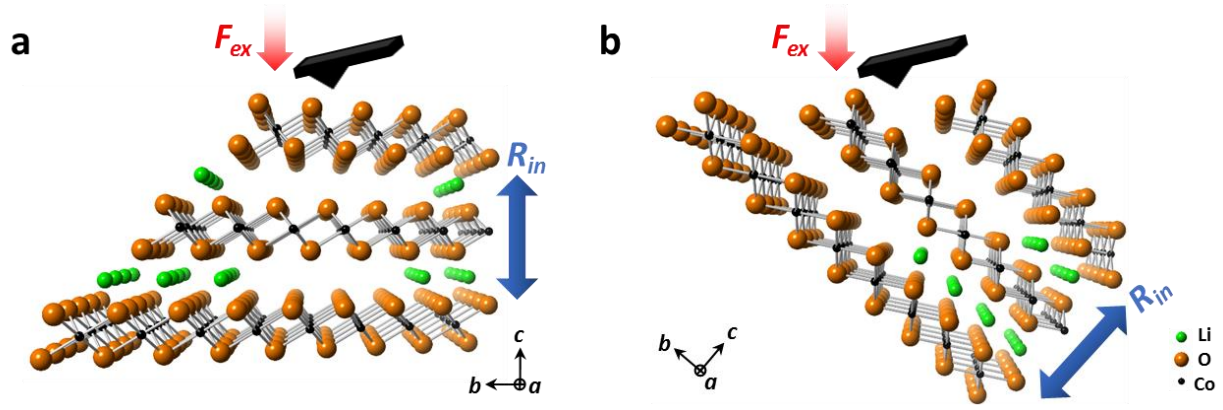

Figure 7. The atomic model of the diffusion of lithium ions inside the layered $LiCoO_2$ cathode with its (001) plane oriented perpendicular to the electric field (a) or close to the electric field (b) under an applied force $\boldsymbol{F_{ex}}$. The repulsive forces between the CoO_2 layers were indicated as $\boldsymbol{R_{in}}$.

If the $LiCoO_2$ grain was oriented with its (001) plane perpendicular to the electric field (Figure 7a), it is possible that the external stress field suppressed the expansion of CoO_2 layers. The electrostatic force between two adjacent CoO_2 layers is close to 4.19 nN, given the 4.68 Å

distance between two adjacent CoO_2 layers.[43] This electrostatic force is relatively small compared with the applied forces. Taking multiple layers of CoO_2 into consideration, when the applied force ($\boldsymbol{F_{ex}}$) is large enough to overcome this repulsive force ($\boldsymbol{R_{in}}$), the expansion of the CoO_2 layers could be suppressed. The actual surface expansion will show the compensation between these two forces. This is consistent with the reduced volume expansion with the linear increase of applied forces, observed along the region h-h' (Figure 6b). However, if the $LiCoO_2$ grain was oriented with its (001) plane close to the electric field (Figure 7b), repulsive forces generated from the deficiency of lithium ions cannot be fully compensated by the external stresses. This would also result in a reduced surface height, which is similar to that observed at g-g' region (Figure 6b). Along with the reduced surface height, a deeper penetration depth of the electric field can be expected, and more lithium ions will be driven away from the layered $LiCoO_2$. This is consistent with the observation that the surface area, R_{max}, and increasing rate of R_a were all reduced when a higher force was applied (Figure 6d).

4. CONCLUSIONS

The study of lithium ion transportation in electrode materials and the influencing factors for this property are critical for the design of high-rate and high-performance lithium ion batteries. Our results reveal that localized mechanical stresses can facilitate the redistribution of lithium ions inside the layered $LiCoO_2$. Conductive AFM tests, combined with the dynamic force ramping technique, demonstrated the applied stress was capable of inducing reversible resistive switching of the layered $LiCoO_2$ cathode. With the suppressed expansion of the CoO_2 layers, a deeper penetration depth of the electric field was proposed to be responsible for the enhanced redistribution of lithium ions and the increased current responses from the $LiCoO_2$ substrate. The

approach presented here offers guidance for future studies of ionic redistribution in other layered materials. Currently, the mechanical stress applied is localized and the forces are limited in nanoscale (20~200nN). Further study of this influencing factor at the higher level or introducing mechanical loading to battery cells during electrochemical cycling would also be beneficial for practical application. Also, if the temperature effect on the redistribution of lithium ions under different stress field can be studied, the thermodynamic driving force of the diffusion of lithium ions can also be estimated quantitatively.

ASSOCIATED CONTENT

Supporting Information

This material is available free of charge via the Internet at http://pubs.acs.org.

SEM and XRD pattern of the polycrystalline $LiCoO_2$ substrate; Variation of the R_q value as a function of applied external forces for the $LiCoO_2$ substrate; Grain orientation effect on the C-AFM current mapping of the $LiCoO_2$ substrate; The representative I/V curves from different spots of the layered $LiCoO_2$; Variation of the R_q value as a function of applied external forces for the HOPG substrate; Electrical current mapping from HOPG substrate; Current response at spot 5 with respect to its tip-sample distance during both trace and retrace processes; Cross-section analysis of the $LiCoO_2$ sample height versus applied stresses.

AUTHOR INFORMATION

Corresponding Author

*E-mail: rsyassar@uic.edu

Notes

The authors declare no competing financial interests.

ACKNOWLEDGMENT

R. Shahbazian-Yassar acknowledges the financial support from the National Science Foundation (Award No. DMR-1620901). W. Yao acknowledges the financial support from China Scholarship Council (CSC, No.201309110076).

ABBREVIATIONS

C-AFM, Conductive atomic force microscopy; HOPG, highly ordered pyrolytic graphite; ESM, electrochemical strain microscopy.

REFERENCES

(1) Tarascon, J.-M.; Armand, M., Issues and Challenges Facing Rechargeable Lithium Batteries. *Nature* **2001,** *414* (6861), 359-367.

(2) Lu, L.; Han, X.; Li, J.; Hua, J.; Ouyang, M., A Review on the Key Issues for Lithium-Ion Battery Management in Electric Vehicles. *J. Power Sources* **2013,** *226*, 272-288.

(3) Smith, K.; Wang, C.-Y., Power and Thermal Characterization of a Lithium-Ion Battery Pack for Hybrid-Electric Vehicles. *J. Power Sources* **2006,** *160* (1), 662-673.

(4) Hosono, E.; Kudo, T.; Honma, I.; Matsuda, H.; Zhou, H., Synthesis of Single Crystalline Spinel $LiMn_2O_4$ Nanowires for a Lithium Ion Battery with High Power Density. *Nano Lett.* **2009,** *9* (3), 1045-1051.

(5) Bruce, P. G.; Scrosati, B.; Tarascon, J. M., Nanomaterials for Rechargeable Lithium Batteries. *Angew. Chem., Int. Ed.* **2008,** *47* (16), 2930-2946.

(6) Nie, A.; Gan, L.-Y.; Cheng, Y.; Asayesh-Ardakani, H.; Li, Q.; Dong, C.; Tao, R.; Mashayek, F.; Wang, H.-T.; Schwingenschlögl, U., Atomic-Scale Observation of Lithiation Reaction Front in Nanoscale SnO_2 Materials. *ACS Nano* **2013,** *7* (7), 6203-6211.

(7) Yuan, Y.; Nie, A.; Odegard, G. M.; Xu, R.; Zhou, D.; Santhanagopalan, S.; He, K.; Asayesh-Ardakani, H.; Meng, D. D.; Klie, R. F., Asynchronous Crystal Cell Expansion During Lithiation of K^+-Stabilized α-MnO_2. *Nano Lett.* **2015,** *15* (5), 2998-3007.

(8) Balke, N.; Jesse, S.; Morozovska, A.; Eliseev, E.; Chung, D.; Kim, Y.; Adamczyk, L.; Garcia, R.; Dudney, N.; Kalinin, S., Nanoscale Mapping of Ion Diffusion in a Lithium-Ion Battery Cathode. *Nat. Nanotechnol.* **2010,** *5* (10), 749-754.

(9) Yuan, Y.; Wood, S. M.; He, K.; Yao, W.; Tompsett, D.; Lu, J.; Nie, A.; Islam, M. S.; Shahbazian-Yassar, R., Atomistic Insights into the Oriented Attachment of Tunnel-Based Oxide Nanostructures. *ACS Nano* **2016,** 10 (1), 539–548.

(10) Kannan, A.; Rabenberg, L.; Manthiram, A., High Capacity Surface-Modified $LiCoO_2$ Cathodes for Lithium-Ion Batteries. *Electrochem. Solid-State Lett.* **2003,** *6* (1), A16-A18.
(11) Kim, Y. J.; Kim, H.; Kim, B.; Ahn, D.; Lee, J.-G.; Kim, T.-J.; Son, D.; Cho, J.; Kim, Y.-W.; Park, B., Electrochemical Stability of Thin-Film $LiCoO_2$ Cathodes by Aluminum-Oxide Coating. *Chem. Mater.* **2003,** *15* (7), 1505-1511.
(12) Motohashi, T.; Sugimoto, Y.; Masubuchi, Y.; Sasagawa, T.; Koshibae, W.; Tohyama, T.; Yamauchi, H.; Kikkawa, S., Impact of Lithium Composition on the Thermoelectric Properties of the Layered Cobalt Oxide System Li_xCoO_2. *Phys. Rev. B* **2011,** *83* (19), 195128.
(13) Xia, H.; Lu, L.; Meng, Y.; Ceder, G., Phase Transitions and High-Voltage Electrochemical Behavior of $LiCoO_2$ Thin Films Grown by Pulsed Laser Deposition. *J. Electrochem. Soc.* **2007,** *154* (4), A337-A342.
(14) Moradpour, A.; Schneegans, O.; Franger, S.; Revcolevschi, A.; Salot, R.; Auban-Senzier, P.; Pasquier, C.; Svoukis, E.; Giapintzakis, J.; Dragos, O., Resistive Switching Phenomena in $LixCoO_2$ Thin Films. *Adv. Mater.* **2011**, 23 (36), 4141-4145.
(15) Amatucci, G.; Tarascon, J.; Klein, L., CoO_2, the End Member of the Li_xCoO_2 Solid Solution. *J. Electrochem. Soc.* **1996,** *143* (3), 1114-1123.
(16) Sun, H.; Liu, Q.; Li, C.; Long, S.; Lv, H.; Bi, C.; Huo, Z.; Li, L.; Liu, M., Direct Observation of Conversion between Threshold Switching and Memory Switching Induced by Conductive Filament Morphology. *Adv. Funct. Mater.* **2014,** *24* (36), 5679-5686.
(17) Sun, J.; Liu, Q.; Xie, H.; Wu, X.; Xu, F.; Xu, T.; Long, S.; Lv, H.; Li, Y.; Sun, L., In Situ Observation of Nickel as an Oxidizable Electrode Material for the Solid-Electrolyte-Based Resistive Random Access Memory. *Appl. Phys. Lett.* **2013,** *102* (5), 053502.
(18) Xu, Z.; Bando, Y.; Wang, W.; Bai, X.; Golberg, D., Real-Time in Situ Hrtem-Resolved Resistance Switching of Ag_2S Nanoscale Ionic Conductor. *ACS Nano* **2010,** *4* (5), 2515-2522.
(19) Chen, X.; Zhu, X.; Xiao, W.; Liu, G.; Feng, Y. P.; Ding, J.; Li, R.-W., Nanoscale Magnetization Reversal Caused by Electric Field-Induced Ion Migration and Redistribution in Cobalt Ferrite Thin Films. *ACS Nano* **2015,** *9* (4), 4210-4218.
(20) Zhu, X.; Ong, C. S.; Xu, X.; Hu, B.; Shang, J.; Yang, H.; Katlakunta, S.; Liu, Y.; Chen, X.; Pan, L., Direct Observation of Lithium-Ion Transport under an Electrical Field in Li_xCoO_2 Nanograins. *Sci. Rep.* **2013,** *3*:1084; DOI:10.1038/srep01084.
(21) Balke, N.; Kalnaus, S.; Dudney, N. J.; Daniel, C.; Jesse, S.; Kalinin, S. V., Local Detection of Activation Energy for Ionic Transport in Lithium Cobalt Oxide. *Nano Lett.* **2012,** *12* (7), 3399-3403.
(22) Balke, N.; Eliseev, E.; Jesse, S.; Kalnaus, S.; Daniel, C.; Dudney, N. J.; Morozovska, A.; Kalinin, S. V., Three-Dimensional Vector Electrochemical Strain Microscopy. *J. Appl. Phys.* **2012,** *112* (5), 052020.
(23) Sader, J. E.; Chon, J. W.; Mulvaney, P., Calibration of Rectangular Atomic Force Microscope Cantilevers. *Rev. Sci. Instrum.* **1999,** *70* (10), 3967-3969.
(24) Mohideen, U.; Roy, A., Precision Measurement of the Casimir Force from 0.1 to 0.9 M M. *Phys. Rev. Lett.* **1998,** *81* (21), 4549-4552.
(25) Brunero Cappella, G. D., Force-Distance Curves by Atomic Force Microscopy. *Surf. Sci. Rep.* **1999,** *34* (1-3), 1-104.
(26) Schneegans, O.; Moradpour, A.; Boyer, L.; Ballutaud, D., Nanosized Electrochemical Cells Operated by AFM Conducting Probes. *J. Phys. Chem. B.* **2004,** *108* (28), 9882-9887.

(27) Schneegans, O.; Moradpour, A.; Dragos, O.; Franger, S.; Dragoe, N.; Pinsard-Gaudart, L.; Chrétien, P.; Revcolevschi, A., Na_xCoO_2: A New Opportunity for Rewritable Media? *J. Am. Chem. Soc.* **2007,** *129* (24), 7482-7483.

(28) Sawada, S.; Tsukiji, S.; Shimada, S.; Tamai, T.; Hattori, Y. Current Density Analysis of Thin Film Effect in Contact Area on Led Wafer. In *Electrical Contacts (Holm), 2012 IEEE 58th Holm Conference.* **2012**, 1-6.

(29) Edman, L.; Sundqvist, B.; McRae, E.; Litvin-Staszewska, E., Electrical Resistivity of Single-Crystal Graphite under Pressure: An Anisotropic Three-Dimensional Semimetal. *Phys. Rev. B* **1998,** *57* (11), 6227-6230.

(30) Vinckier, A.; Semenza, G., Measuring Elasticity of Biological Materials by Atomic Force Microscopy. *FEBS Lett.* **1998,** *430* (1), 12-16.

(31) Volodin, A.; Ahlskog, M.; Seynaeve, E.; Van Haesendonck, C.; Fonseca, A.; Nagy, J., Imaging the Elastic Properties of Coiled Carbon Nanotubes with Atomic Force Microscopy. *Phys. Rev. Lett.* **2000,** *84* (15), 3342-3345.

(32) Eskelsen, J. R.; Qi, Y.; Schneider-Pollack, S.; Schmitt, S.; Hipps, K.; Mazur, U., Correlating Elastic Properties and Molecular Organization of an Ionic Organic Nanostructure. *Nanoscale* **2014,** *6* (1), 316-327.

(33) Trtik, P.; Kaufmann, J.; Volz, U., On the Use of Peak-Force Tapping Atomic Force Microscopy for Quantification of the Local Elastic Modulus in Hardened Cement Paste. *Cem. Concr. Res.* **2012,** *42* (1), 215-221.

(34) Tsuji, T.; Yamanaka, K., Observation by Ultrasonic Atomic Force Microscopy of Reversible Displacement of Subsurface Dislocations in Highly Oriented Pyrolytic Graphite. *Nanotechnology* **2001,** *12* (3), 301-307.

(35) Bhushan, B.; Kwak, K. J.; Palacio, M., Nanotribology and Nanomechanics of AFM Probe-Based Data Recording Technology. *J. Phys.: Condens. Matter* **2008,** *20* (36), 365207.

(36) Koren, E.; Knoll, A.; Lörtscher, E.; Duerig, U., Direct Experimental Observation of Stacking Fault Scattering in Highly Oriented Pyrolytic Graphite Meso-Structures. *Nat. Commun.* **2014,** *5*:5837; DOI:10.1038/ncomms6837.

(37) Qu, M.; Woodford, W. H.; Maloney, J. M.; Carter, W. C.; Chiang, Y. M.; Van Vliet, K. J., Nanomechanical Quantification of Elastic, Plastic, and Fracture Properties of $LiCoO_2$. *Adv. Energy Mater.* **2012,** *2* (8), 940-944.

(38) Van der Ven, A.; Ceder, G., Lithium Diffusion in Layered $LixCoO_2$. *Electrochem. Solid State Lett.* **2000,** *3* (7), 301-304.

(39) Ben Yahia, H.; Shikano, M.; Kobayashi, H., Phase Transition Mechanisms in $LixCoO_2$ ($0.25 \leq x \leq 1$) Based on Group – Subgroup Transformations. *Chem. Mater* **2013,** *25* (18), 3687-3701.

(40) Gao, Y.; Zhou, M., Strong Stress-Enhanced Diffusion in Amorphous Lithium Alloy Nanowire Electrodes. *J. Appl. Phys.* **2011,** *109* (1), 014310.

(41) Daw, M. S.; Windl, W.; Carlson, N. N.; Laudon, M.; Masquelier, M. P., Effect of Stress on Dopant and Defect Diffusion in Si: A General Treatment. *Phys. Rev. B* **2001,** *64* (4), 045205.

(42) Shao, W.; Gan, Z.; Mhaisalkar, S.; Chen, Z.; Li, H., The Effect of Line Width on Stress-Induced Voiding in Cu Dual Damascene Interconnects. *Thin Solid Films* **2006,** *504* (1), 298-301.

(43) Shao-Horn, Y.; Croguennec, L.; Delmas, C.; Nelson, E. C.; O'Keefe, M. A., Atomic Resolution of Lithium Ions in $LiCoO_2$. *Nat. Mater.* **2003,** *2* (7), 464-467.

Table of Contents Graphic